[20] L. Blackmore and M. Ono, “Convex chance constrained predictive control without sampling,” in *Proc. AIAA Guid., Navigat. Control Conf.*, 2009, p. 14.
[21] M. Ono and B. Williams, “An efficient motion planning algorithm for stochastic dynamic systems with constraints on the probability of failure,” in *Proc. AAAI Conf. Artif. Intell.*, 2008, pp. 1376–1382.
[22] K. B. Petersen and M. S. Pedersen. (Nov. 2008). Matrix cookbook [Online]. Available: www.matrixcookbook.com
[23] S. Thrun, W. Burgard, and D. Fox, *Probabilistic Robotics*. Cambridge, MA: MIT Press, 2005.

Modeling and Evaluation of Low-Cost Force Sensors

C. Lebossé, P. Renaud, B. Bayle, and M. de Mathelin

***Abstract*—Low-cost piezoresistive sensors can be of great interest in robotic applications due not only to their advantageous cost but to their dimension as well, which enables an advanced mechanical integration. In this paper, a comparison of two commercial piezoresistive sensors based on different technologies is performed in the case of a medical robotics application. The existence of significant nonlinearities in their dynamic behavior is demonstrated, and a nonlinear modeling is proposed. A compensation scheme is developed for the sensor with the largest nonlinearities before discussing the selection of a sensor for dynamic applications. It is shown that force control is achievable with these kinds of sensors, in spite of their drawbacks. Experiments with both types of sensors are presented, including force control with a medical robot.**

***Index Terms*—Force control, nonlinear modeling, piezoresistive sensors.**

I. Introduction

In the field of robotics, force control is needed to ensure safety and comfort in human/robot interaction, for instance, in medical robotics applications [2], [3]. An increasingly number of industrial [4] and service [5] robotic applications are also concerned by close human/robot interactions and force control. For these applications, low-cost, easy-to-integrate force sensors are becoming very necessary.

Over the past two decades, sensors such as Interlink Force Sensing Resistor (FSR), Tekscan Flexiforce, or Peratech QTC have been developed using novel piezoresistive effects [6]–[8]. Even though these low-cost sensors exhibit a lower accuracy than other types of sensors, they combine interesting dimensions with a very small thickness and a high flexibility that facilitates their integration, and it has been demonstrated that some sensors like the Flexiforce are insensitive to magnetic fields [9]. For a growing number of medical applications involving the placement of the patient inside a Magnetic Resonance Imaging (MRI) scanner [10] or in pulsed magnetic fields [3], these sensors seem to be well adapted to force-control tasks and have already been considered in control schemes [11]–[13].

Manuscript received May 5, 2010; revised November 19, 2010; accepted February 17, 2011. Date of publication April 5, 2011; date of current version August 10, 2011. This paper was recommended for publication by Associate Editor S. Hirai and Editor G. Oriolo upon evaluation of the reviewers' comments. This paper was presented in part at the 2008 IEEE International Conference on Robotics and Automation, Pasadena, CA.

C. Lebossé is with Luxscan Technologies, L-4384 Ehlerange, Luxembourg (e-mail: cyrille_lebosse@yahoo.fr).

P. Renaud, B. Bayle, and M. de Mathelin are with the Laboratoire des Sciences de l'Image de l'Information et de la Télédétection, Centre National de la Recherche Scientifique, Strasbourg University, 67412 Illkirch, France (e-mail: pierre.renaud@insa-strasbourg.fr; bernard@eavr.u-strasbg.fr; demathelin@unistra.fr).

Color versions of one or more of the figures in this paper are available online at http://ieeexplore.ieee.org.

Digital Object Identifier 10.1109/TRO.2011.2119850

Fig. 1. Robotic system and its end-effector with the embedded force sensor.

Therefore, several researchers have proposed a characterization of low-cost piezoresistive force sensors. Although static properties have always been evaluated [14]–[16], only a few authors have considered their response to dynamic loading. In [17], the hysteresis of the sensor output is assessed when the sensor is submitted to a dynamic load. Otto *et al.* [18] have shown that Tekscan K-Scan sensors exhibit a very strong time drift that is responsible for large errors when the sensors are submitted to harmonic loading. A compensation scheme is then proposed. It performs a deconvolution using Boltzmann heredity integral, which was developed in the context of viscoelasticity of materials [19]. Komi *et al.* [20] analyzed the Tekscan 9811, the Interlink Flexiforce, and the Peratech QTC sensors when submitted to sinusoidal loads. The evolution of the sensors output is evaluated in terms of time drift. The authors observed that this drift can be significant since the sensor output decreases by 10% in 5 s. The duration of the experiments, however, remains shorter than 1 min, which is not sufficient for many applications. For example, the analysis of prostheses behavior in biomechanics or the compensation of breathing motion by force control in medical robotics applications require much longer experiments.

In the following, robotized transcranial magnetic stimulation (TMS) is considered [3]. In this medical application, a magnetic stimulation coil located at the end-effector of the robotic system (see Fig. 1) has to be placed in contact with the head of the patient. Therefore, force control is needed, which prevents any air gap between the coil and the patient's head, guarantees the safety of the patient as well as his comfort, and enables the compensation of the patient's movements. The maximum contact force must remain below 5 N during a typical 20-min treatment. The contact of the coil on the head can be continuous, in the case of repetitive stimulation, or discontinuous, in the case of some protocol like the cortex mapping using single-pulse stimulations. Furthermore, the contact of the coil on the head can be discontinued after sudden head movements. During the treatment, the sensor loading will vary due to the patient movements. Low-cost piezoresistive sensors offer an interesting solution for force measurement in this context, because of their dimensions and their immunity to magnetic fields.

In this paper, the focus is put on two widespread commercial low-cost piezoresistive sensors: the Tekscan Flexiforce and the Interlink FSR, like in [1]. The existence of strong nonlinearities in their dynamic response is outlined, and the opportunity to compensate for

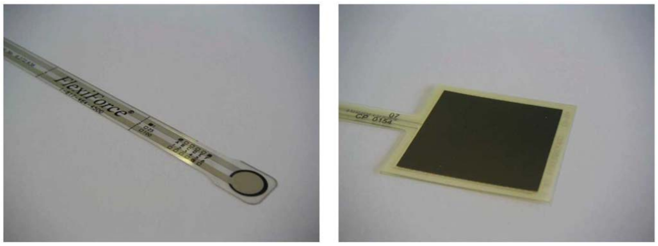

Fig. 2. (Left) Tekscan Flexiforce and (right) Interlink FSR.

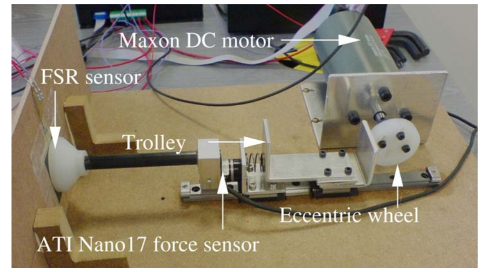

Fig. 3. Force sensors test bench during the evaluation of the FSR sensor.

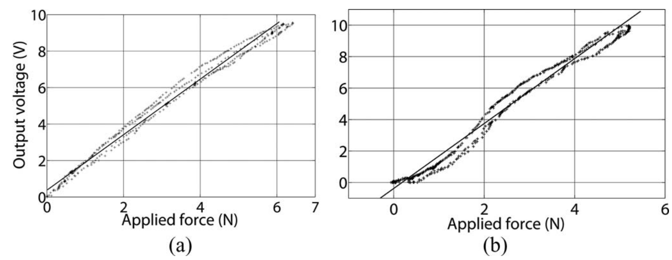

Fig. 4. Calibration of both sensors. The identified model is represented by the continuous line. (a) Flexiforce sensor. (b) FSR sensor.

these nonlinearities is discussed. A comparison of the sensors respective merits, with possible applications, is proposed with an experimental validation of force-control schemes using these sensors. The paper is organized as follows. The sensors and the experimental setup are presented in Section II. Static properties are briefly given in Section III, and the nonlinearity of the Tekscan Flexiforce and the Interlink FSR is shown. Then, the nonlinear modeling of the Flexiforce sensor, which exhibits the most-significant nonlinearities, is developed in Section IV, with validation by force-control experiments. Finally, the choice of a sensor for force-control applications is discussed in Section V. Force-control experiments for the TMS medical application are also presented in this last section.

II. Sensors and the Experimental Setup

A. Evaluated Sensors: Tekscan Flexiforce and Interlink FSR

For the Tekscan Flexiforce sensor, a semiconductive ink is located between two thin polyester sheets covered with a conductive material. The ink is pressure-sensitive, and therefore, an electrical-resistance variation is obtained when a force is applied on the round-shape active area, which is located at the tip of the sensor (see Fig. 2). Its resistance decreases with the applied load. To measure forces, according to the manufacturer's specifications [21], the sensor is integrated in a circuit as a variable resistor. A linear analog-voltage variation is then obtained with respect to the applied force.

The FSR sensor is based on a different piezoresistive effect. This thin film device consists of two conducting interdigitated patterns deposited on a thermoplastic sheet, which faces another sheet containing a conductive polyetherimide film. A spacer placed between the sheets allows the two sheets to make electrical contact when a force is applied. In the unloaded state, the sensor has an infinite conductance. As the applied force increases, the two layers compress each other, increasing the contact area and decreasing the electrical resistance. Unlike the Flexiforce sensor, no specification is given by the manufacturer about its linearity. The FSR sensor is originally dedicated to contact detection; however, it is mentioned in the manufacturer's specifications [22] that a linear force/conductance relationship can be expected. This sensor is considered hereafter for more advanced applications using the same implementation than for the Flexiforce.

These sensors can be manufactured with different force-measurement ranges, and with sensing areas of different shapes. A maximum force of 5 N is expected for the TMS medical application. Flexiforce A-201 and FSR SS-U-N-S45, which are manufactured under license by the IEE, have been selected. Indeed, the former has a force range of 4.5 N, and the latter has a maximum force range of 100 N. The adaptation of the force range is possible with the selection of an adequate resistance in the electrical circuit. The selected model of Flexiforce sensor has a sensing area with a 10-mm-diameter circular shape, and the FSR sensor has a sensing area with a 38 mm × 38 mm square shape.

B. Experimental Setup

The static and dynamic properties of the sensors are assessed with the experimental setup presented in Fig. 3. An eccentric wheel is mounted on a Maxon DC motor F2260 that induces the movement of a trolley on a linear guide. The eccentricity of the wheel can be adjusted to a value between 0 and 12 mm. The movement is converted into a force applied on the sensors by means of a spring of stiffness approximately equal to 0.25 N/mm. Nonmetallic elements are used at proximity of the sensors, so that it could be verified that both sensors are insensitive to the magnetic field delivered by the TMS stimulation coil.

The test bed is assembled to ensure a constant pressure on the active area of the sensors, in order to strictly follow the sensor manufacturer's recommendations. The velocity-controlled motor induces, by means of the spring, forces in the range of $[0, 5\mathrm{N}]$. A direct force measurement is simultaneously performed using an ATI Nano17 force sensor. The Nano17 has a resolution of 0.025 N and a high bandwidth that exceeds 200 Hz [23].

III. Sensor Selection for Dynamic Applications

In this section, static and dynamic properties of the Flexiforce and FSR sensors are given.

A. Static Evaluation

For both sensors, the reference resistance in the measurement circuit is selected in order to obtain a 0–10 V output voltage in the 0–5-N force range. Each force sensor is calibrated manually by continuously applying the force range twice. A linear model is identified as

$$F = GU + F_0 \tag{1}$$

where G and F_0, respectively, stand for the gain and the offset of the sensor, U is the measured output voltage, and F is the actual applied force.

Typical calibration curves are presented in Fig. 4. The value of the departure from linearity, the hysteresis with respect to the full scale, and the repeatability are indicated in Table I for both the sensors.

TABLE I
STATIC PROPERTIES OF THE FLEXIFORCE AND FSR SENSORS

	Error of Linearity	Hysteresis	Repeatability	Time drift
Flexiforce	5%	10%	3.6%	6%
FSR	7%	8%	2.1%	4%

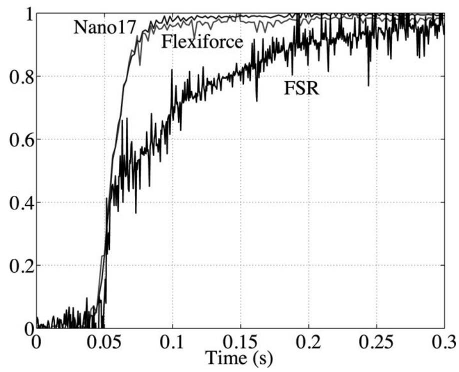

Fig. 5. Step responses of the Nano17, FSR, and Flexiforce sensors. The responses are normalized with respect to the final value for the comparison.

Repeatability is evaluated by computing the mean error when applying ten times ten different loads. The Flexiforce sensor is characterized by a better linearity than the FSR, which is as expected from the specifications of the sensors manufacturers. In terms of repeatability, hysteresis, and time drift, the FSR and Flexiforce have very close performances. The measured static properties are similar to those indicated in [14], [15], and [20]. Small differences can be observed; however, these previously published results do not consider the same force range. It is worth noticing that both sensors exhibit a small time drift, i.e., below 6% for 20 min, which is the required duration of our application. For some other piezoresistive sensors, time drift can be a major limitation. According to Otto *et al.* [18], a variation of more than 30% of the sensor output voltage is observed after 10 min in the case of the Tekscan K-Scan.

B. Step Response

For force-control applications, the dynamic behavior also has to be taken into account.

A step input is applied to the velocity controller of the motor in the experimental setup. Even if the actual force applied to the sensors is not a true step, due to the eccentric-wheel profile and the time constant of the motor, this experiment allows very different behaviors to be observed (see Fig. 5). The Flexiforce sensor reaches the final value in 70 ms, which is approximately the time needed by the Nano17 that can be considered as the reference. On the contrary, the FSR sensor needs 210 ms to reach the final value. Consequently, the bandwidth of the Flexiforce sensor seems to be much higher than the FSR bandwidth.

C. Harmonic Response

Considering the static properties and the step response, the Flexiforce seems to be the most-appropriate sensor for force control. However, this is no longer true when a simple harmonic load is applied. The sensor responses do not present a significant attenuation for frequencies up to 4 Hz. However, nonstationary responses can be observed. A strong decline of the sensor responses occurs after a few seconds of sinusoidal excitation. This phenomenon is much more significant for the Flexiforce sensor, as emphasized in Fig. 6, where typical sensor responses are given.

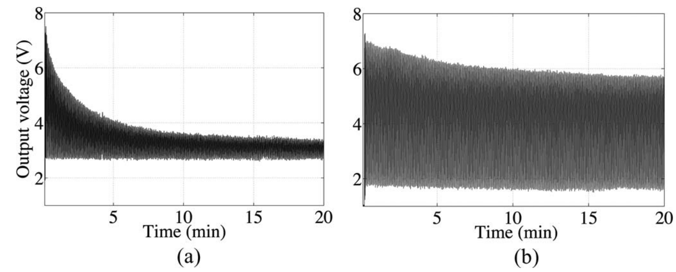

Fig. 6. Sensor responses for a sinusoidal load applied during 20 min with a force range between 1.3 and 4.4 N and a frequency of 0.25 Hz. (a) Flexiforce sensor. (b) FSR sensor.

Only the maxima of the sensor response decrease with time, with the minima remaining at the same level. For the Flexiforce sensor, the decrease is rather exponential with a loss that can reach 90% of the sensor initial response after 20 min, depending on the force range and the frequency. In the case of the FSR sensor, the decrease is rather linear with a loss that can reach 30%. On average, the signal decrease is equal to 83% for the Flexiforce sensor and 16% for the FSR sensor for sinusoidal excitations of frequency, amplitude, and mean value reported in Table II in Appendix. This phenomenon is even more significant than it appears, even with very low excitation frequencies and force ranges: With the Flexiforce, a loss of 80% (respectively, 70%) can be observed in 20 min with an excitation of 1.5 N (respectively, 0.4 N) in amplitude and only 0.05 Hz (respectively, 0.5 Hz) in frequency.

As outlined in Section I, only a few authors have considered the dynamic behavior of these sensors. To our knowledge, the aforementioned strong nonlinearities of the sensors when submitted to sinusoidal loads have never been described. Komi *et al.* [20] considered sine waves for the reference value, and in Fig. 8 of their paper, it is remarked that the Flexiforce output presents the signal decrease described in this section. However, only 5-s experiments have been considered in [20] so that the signal decrease is interpreted as a linear time drift. Komi *et al.* [20] further observed that the drift varied significantly between experiments, which probably denotes that the sensor output is a function of the amplitude and of the frequency of the excitation and that a parametric model is needed to quantify the nonlinearities.

D. Variations of the Sensor Static Properties

Due to the variability of the behavior of the sensors, the gain and offset introduced in (1) present noticeable variations. The relative standard deviation of the gain and the offset of a Flexiforce sensor have been experimentally evaluated to 9% and 22%, respectively, whereas they are equal to 10% and 45%, respectively, for an FSR sensor. These values are consistent for several specimens of each sensor.

The dynamic loading of the sensors has also an influence on the sensors gain. On average, the gain of the Flexiforce sensors is increased by 7% with a 20-min sinusoidal excitation. On the contrary, the FSR sensor gain decreases by 11% on average.

An increase in the static gain means a lower sensor output voltage for a given force. Therefore, the gain variation of the Flexiforce sensors tends to lower the output voltage simultaneously to the decrease of the sensor response due to the dynamic loading. On the contrary, the static-gain variation of the FSR sensor induces an increase of the sensor-output voltage, which tends to oppose the sensor signal decrease due to a dynamic loading. As a consequence, the precise modeling of this latter sensor (see [1]) is very tedious. The accuracy of the compensation obtained after modeling may be unsatisfactory to compensate for its default. Indeed, the shape of the signal delivered by an FSR

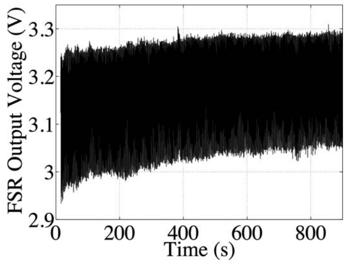

Fig. 7. FSR sensor output voltage for a sinusoidal load of mean value 3.5 N, amplitude 0.4 N, and frequency 0.5 Hz.

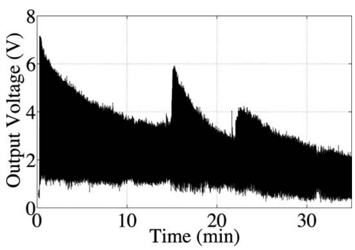

Fig. 8. Flexiforce output voltage for a sinusoidal load of frequency successively equal to 0.5, 2, and 3 Hz.

sensor is somewhat erratic; the signal maxima decreased in most of the experiments, but a signal increase can sometimes be observed (see Fig. 7).

In conclusion, since the FSR sensor exhibits much less dynamic drawbacks than the Flexiforce sensor, and since its nonlinearities cannot be accurately modeled, we propose to use it without compensation. On the contrary, the Flexiforce sensor needs to be modeled, in order to compensate for the output signal decrease, as developed in the next section.

IV. Modeling and Compensation of the Flexiforce

A. Nonlinear Modeling

Experimental observations show that the underlying physical effects are complex. The behavior is nonstationary, and a knowledge-based model is out of reach. Thus, no physical *a priori* knowledge is used for the model identification. In order to obtain a model of the Flexiforce, an harmonic excitation has been performed in two steps.

1) Load Composed of a Single Sine Wave

a) Modeling: First, the sensor response to a single harmonic excitation is modeled. Let f, A, and m, respectively, stand for the frequency, the amplitude, and the mean value of the applied force

$$F = A\sin(2\pi f t) + m \tag{2}$$

with $m \geq A$ to ensure a continuous contact on the sensor.

For the sake of simplicity, a decoupled influence of the three parameters (m, A, f) is assumed, and three series of experiments are performed, with each one corresponding to the variation of only one parameter. The range for the mean value and the amplitude is selected in order to handle any excitation between 0 and 4.5 N, i.e., in the Flexiforce force range. Frequencies between 0 and 4 Hz are chosen, considering the fact that the signal loss is already very important for such frequencies and is not relevant to go beyond that range. For such a frequency range, no significant phase shift is observed. Time horizons of 20 min are considered.

According to the observations in Section III-C, the value of the minima $U_{\min}$ of the sensor output voltage remains constant, while an exponential decrease best describes the signal maxima drift. The following model is used for the maxima of the output-voltage response:

$$U_{\max} = U_{\max}(t) = U_{\min} + ae^{-bt} + c \tag{3}$$

with $a,\ b,\ c > 0 \in \mathbb{R}$, and $U_{\min}$ inferred from (1) and (2):

$$U_{\min} = \frac{m - A - F_0}{G}. \tag{4}$$

It is important to note that the variations of the gain and the offset evoked in Section III-D have a significant influence on the computation of $U_{\min}$ in (3). As a consequence, the dynamic effects may be incorrectly evaluated.

b) Identification: Hereafter, our purpose is to establish a model for compensation that can be identified for a given type of sensor and that can be used for compensation without a complete identification process of each sensor specimen. The experiments have been performed using four different specimens. Therefore, the accuracy of the model depends both on the repeatability error of each specimen and on the variability between sensors. The overall variability between specimens is significant, i.e., the parameter b presents a variation of approximately 25% when different specimens are tested in the same experimental conditions.

In Appendix Table II presents the variations of the parameters a, b, and c due to f, A, and m, as well as the root-mean-square error (RMSE, as defined in the Appendix) for the identification of the response maxima. From the analysis of these variations, three parameter-variation laws are inferred:

$$\begin{aligned} a &= 0.884A^2 + 0.865A \\ b &= 0.0019f + 0.0056 \\ c &= \frac{1}{1 + 1.377A^2}a. \end{aligned} \tag{5}$$

The parameter a is expressed as a function of the amplitude A only, with $a = 0$ when $A = 0$, i.e., when no sine load is applied. A quadratic model best fits the experimental results. The parameter b, which describes the rate of decrease, is best described as a linear function of the frequency f only, even though a constant value may be used in practice. Finally, the ratio c/a that is linked to the output-signal loss is best described by a decreasing function of the amplitude A.

The maxima $U_{\max}$ of the sensor output are estimated with a mean relative error (MRE) of 13% (for the definition of MRE, see the Appendix) on all the data used for the identification. The parameters a, b, and c are obtained by curve fitting from the experimental data using least-square minimization and are computed using the proposed models [see (5)] with average relative errors of, respectively, 17%, 30%, and 14% on the four different specimens. The relatively poor accuracy of the estimation of parameter b should be compared with the previously mentioned variation of 25%. Parameter a describes the maximum value of the initial sensor responses and parameter c the final value of the maxima, when $t \to \infty$. The accuracy of the estimation of a and c should be compared with the variation of the static gain and offset, which is used to evaluate $U_{\min}$ in (3) and can be considered as good.

c) Cross-validation: On six additional independent datasets, the MRE on the maximal values of the sensor output $U_{\max}(t)$ is equal to 9%. Relative errors on the parameters (a, b, c) are equal, on average, to 9%, 30%, and 18% The accuracy of the introduced nonlinear model with cross-validation data is, therefore, satisfactory. Relative errors in the estimation of the parameters are comparable with the errors introduced by the lack of repeatability of the sensors and the differences of behavior between sensor specimens.

2) Loads With Rich and Time-Varying Frequency Content: The model of (3) can correctly describe the decrease of the maxima of the Flexiforce, even if more complex signals are applied.

a) Sweep signal—First, let us consider a sweep signal with varying frequencies. Curve fitting exhibits acceptable results if the parameters are estimated using (5), with f equal to the initial frequency of the sweep signal. The relative errors in the estimation of a, b, and c, and the MRE in the estimation of $U_{\max}$ are, respectively, equal to 16%, 40%, 32%, and 15% for a sweep signal with ascending frequency between 0 and 3 Hz in 20 min, and 17%, 14%, 4%, and 5% with a descending frequency.

b) Sum of two sinusoids: To study the influence of the parameters in the case of a load with rich frequency content, a sum of two sinusoidal signals is considered as

$$F = A_1 \sin(2\pi f_1 t) + A_2 \sin(2\pi f_2 t) + m \tag{6}$$

without taking into account the mean value of each signal, since the models identified in Section IV-A1 are not a function of the force mean value. The amplitude of the resulting signal depends on the frequencies f_1 and f_2. The expressions of a and c/a introduced in (5) describe, in a satisfactory manner, the observed sensor output decrease if the amplitude of the signal resulting from the sum of the two sinusoidal signals is considered (see Table III in Appendix). The relative errors in the estimation of a and c are, respectively, equal to 28% and 8%. The parameter b can be expressed from the model when considering the lowest frequency in the signal, which is logical as it corresponds to the slowest output decrease. The relative error in the estimation of b is equal to 28% (see Table III in Appendix).

c) More complex signals: Other signals have been considered as cross-validation data to evaluate the model. A load composed of four sinusoidal signals has been applied to the sensor, with the amplitude and frequency of each signal being equal to (0.1 N, 1 Hz), (0.2 N, 0.5 Hz), (0.3 N, 0.1 Hz), and (0.4 N, 0.05 Hz). Taking into account the amplitude of the obtained signal, and the lowest frequency contained in the signal, parameters a, b, and c can be estimated with errors, respectively, equal to 32%, 16%, and 6%. The maxima of the sensor output are described with an MRE equal to 6%.

Considering a pseudo random binary signal with a spectrum range from 0 to 5 Hz ($A = 1.6$ N, $m = 2.6$ N), the sensor behavior is also well identified, with an MRE on the maxima equal to 8% and relative errors on the parameters a, b, and c of, respectively, 27%, 40%, and 3%.

To summarize, in the case of a load with time-varying-frequency content, the lowest frequency of the signal at the beginning of the sensor excitation and the signal amplitude allows description of the sensor dynamic response when introduced in the models given by (5).

3) Other Nonstationary Behaviors: The proposed model can have a reduced efficiency in two situations. First, the sensor behavior is temporarily affected by discontinuities in the signal-frequency content. Indeed, the decrease of the sensor output is affected by an instantaneous modification of the frequency of a sinusoidal load applied to the sensor (see Fig. 8). One can observe a sudden sensor-output increase and then a return to the curve that would have been obtained without the presence of the discontinuity. In order to use the proposed model for compensation, it would be necessary to filter these discontinuities. Second, the sensor does not immediately recover its initial properties when the excitation is stopped. Experiments show that almost 2 h are necessary after 20 min of sensor excitation. If the sensor is used before this rest time, the static gain and offset are modified, within the margins given in Section III-D. The model accuracy will be affected by these errors in the estimation of the sensor behavior.

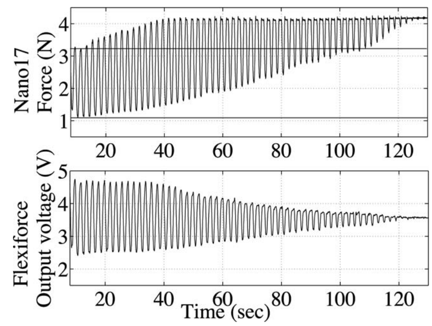

Fig. 9. Force measured with the Nano17 and Flexiforce sensors during a force-control experiment without compensation. Minima and maxima of the reference signal are represented by the horizontal lines.

B. Compensation

1) Principle: The sensor behavior is defined by a simple model [see (3) and (5)], which allows an easy correction of force measurement. The lowest frequency $f_{\min}$ of the output voltage has to be estimated at the beginning of the excitation using a Fast Fourier Transform (FFT). At that time, the sensor maxima are not yet strongly affected by the nonlinearities; therefore, the amplitude A of the force applied to the sensor can be directly extracted. Then, an estimation $\tilde{F}$ of the force F applied to the sensor can be computed using the linear model in (1)

$$\tilde{F} = G\left(\frac{1 + (c/a)}{e^{-bt} + (c/a)}(U - U_{\min}) + U_{\min}\right) + F_0 \tag{7}$$

where a, b, and c are the parameters expressed in (5). The ratio $(1 + c/a)/(e^{-bt} + c/a)$ allows the compensation of the signal decrease; it varies between 1, at the initial instant, and $1 + (a/c)$ when $t \to \infty$.

2) Validation With Force-Control Experiments: The experimental setup shown in Fig. 3 is used with a sensor specimen that is not used for identification. The force-control scheme is very simple as the system is both stable and slow. In the following two cases are considered: 1) The raw-force measurement is compared with a force reference, and the motor control is then obtained using an integral control [1]; 2) the force estimate is computed from (7) and fed back instead of the direct measurement. In both cases, a harmonic force reference is considered that ranges from 1.1 to 3.2 N with a frequency equal to 0.5 Hz.

First, force control without compensation is considered. In Fig. 9, the measurements of the Nano17 and the Flexiforce sensors are represented. When the maxima of the Flexiforce sensor decrease, the controller induces a greater rotation of the eccentric wheel to apply a greater force. This leads to the rise of the maxima that is recorded with the Nano17. However, the controller is not able to compensate the whole range of the sensor-output decrease, and a positive error is cumulated, thereby leading to a rise of the minima as well. Finally, saturation is reached when the extreme position of the wheel is attained. After only 150 s, the eccentric wheel stops and remains in a constant position.

Second, force control is achieved with compensation of the sensor nonlinearities according to (7). Figs. 10 and 11 show the responses obtained when the proposed model is used to compensate for the nonlinearities. Due to the compensation, the force recorded by the Nano17 almost corresponds to the desired force, after some settling time for the maxima, while the minima remain always constant. The amplitude of the eccentric-wheel rotation remains approximately equal to 360°, and the force control is correctly ensured unlike the previous experiment. Moreover, the MRE on the maxima and minima are, respectively,

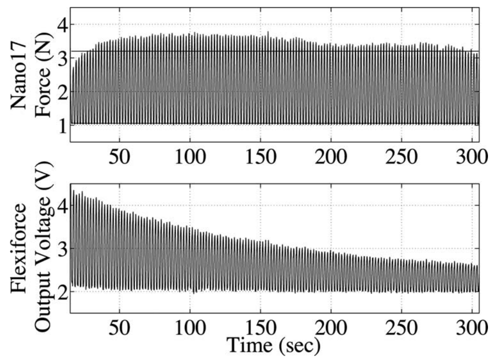

Fig. 10. Force measured with the Nano17 and Flexiforce sensors during a force-control experiment with compensation. Minima and maxima of the reference signal are represented by the horizontal lines.

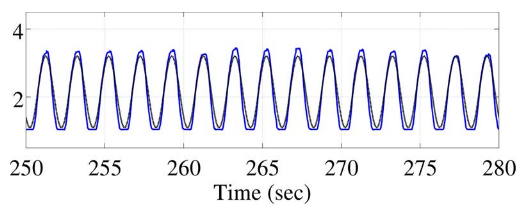

Fig. 11. Closeup on the force measured with the Nano17 during a force-control experiment with compensation. (Black) Reference value.

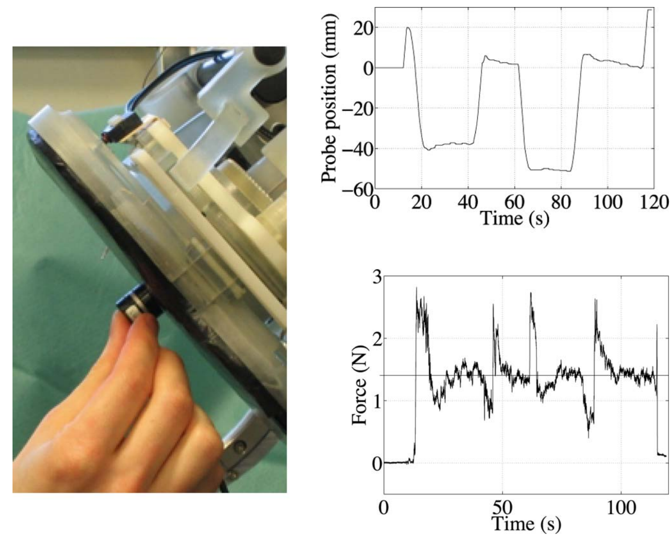

Fig. 12. (Left) Force-control experiment with the TMS robot. (Right) (Up) Position and (Bottom) force applied on the TMS coil measured with the Nano17 sensor.

equal to 4.5% and 7.5% only. The differences between the measured force and the reference value, as observable in Fig. 10, are due to the compensation error and the control error.

The compensation remains efficient during 20-min experiments, with more complex profiles of reference force. For evaluation purposes, a sum of four sinusoidal signals of amplitudes and frequencies equals (0.1 N, 1 Hz), (0.2 N, 0.5 Hz), (0.3 N, 0.1 Hz), and (0.4 N, 0.05 Hz) is considered as the reference force. With the compensation model, even though the amplitude of the signal given by the Flexiforce is divided by a factor 2.5 in 20 min, the force applied to the sensor remains close to the reference. At the end of the experiment, relative errors in the estimation of the minima and maxima of the force measured with the Nano17 are, respectively, equal to 18% and 15%.

V. Which Sensor for Force Control?

In this section, the choice of the most-adequate solution, i.e., either the FSR sensor without compensation or the Flexiforce sensor with compensation, is debated, depending on the application.

A. Flexiforce Versus FSR

The different experimental results highlight that the minima of the sensor response to a dynamic loading can be correctly described by the static model given in (1) for both FSR and Flexiforce sensors. Most of the time, the FSR sensor exhibits a decrease of the response maxima, which, on average, equals to 16%. With the proposed nonlinear model, the minima of the Flexiforce response can also be described with an MRE below 15%, based on all our experimental results. This means that the Flexiforce sensor can be used, after proper modeling and compensation, with similar performances as that of the FSR.

However, the Flexiforce has two more drawbacks that can limit its use. The sensor response to discontinuous forces needs a filtering of the signal that will lead to a decrease in the accuracy of the compensation. Furthermore, the static model that is used in the compensation scheme is also affected by the loading of the sensor, since initial properties of the sensor are recovered after a long time of rest.

On the positive side, the Flexiforce sensor presents a shorter response time and interesting static properties, in particular, a better linearity. Hence, this sensor seems adequate for applications with quasi-static conditions, e.g., when contact must be ensured between a robot and a fixed element. On the contrary, if force control must be performed between a robotic system and an element that exhibits a periodic motion, the FSR sensor seems to be the best choice. The Flexiforce is of interest in this latter dynamic situation only if a permanent contact on the sensor is ensured, no strong discontinuities in the signal are expected, and if the proposed compensation is used.

B. Force Control for Robotized Transcranial Magnetic Stimulation

For robotized TMS, which is our application of interest, several criteria were considered to select the FSR sensor. First, the contact on the sensor can be discontinuous because of the protocol or the possible motions of the patient. Second, the required accuracy of the force servoing is limited. The desired pressure on the patient's head can slightly vary without noticeable effect. It is considered that a force of about 1.5 N remains comfortable for the patient. Finally, as the application is dedicated to medical treatments, the most simple (and then, potentially the more reliable) control technology is certainly preferable. As a consequence, the FSR sensor seems to be the best choice. Force control has been implemented, and a short illustration is given in Fig. 12. A force is applied manually on the FSR sensor. The robot motion in the direction normal to the coil is driven by the force control, and since the structure is decoupled, only 1 degree of freedom is concerned with the contact-force control. The TMS coil position is given in Fig. 12. The force on the FSR sensor is applied using a Nano17 sensor, thus allowing the force to be independently evaluated during the experiment. Finally, the resulting measurements show transients when the pressure is increased or decreased. During time periods with rather constant pressure, the position of the coil barely changes. In the meantime, force noise, as felt by the patient, remains limited, i.e., below 0.34 N.

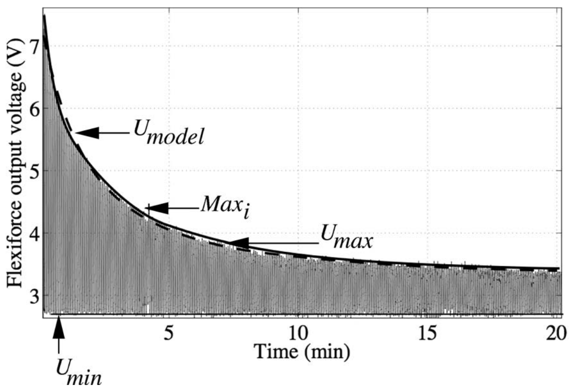

Fig. 13. Curve fitting of the Flexiforce output maxima.

VI. Conclusion

In this paper, low-cost piezoresistive sensors have been studied, with a particular focus on their use for force control. Though generally not considered for that peculiar application, such sensors are very interesting, in particular, because of their cost, their size, and the fact that they are insensitive to magnetic fields. To rule on their adequacy for force-control applications, an extensive characterization of the static and dynamic performances of the Flexiforce and FSR sensors has been performed.

The Flexiforce sensor exhibits better static performances, in particular, a better linearity. However, under dynamic loads, the FSR sensor behaves far better, though both sensors suffer from nonlinearities. This paper shows that the Flexiforce sensor can still be used with dynamic loads, if a modeling and identification is performed, and an adequate compensation scheme is implemented. This has been emphasized by a force-control experiment with the Flexiforce sensor.

Recommendations are done for the use of both sensors, and it is clear that their use in robotic applications should be further investigated. To provide a convincing application, the FSR sensor has been implemented for the control of probe/head contact for robotized TMS, as briefly described at the end of this paper. Other perspectives to this study could include a cross-research effort with physicists or fluid-mechanics engineers to improve the understanding of the observed phenomena.

Appendix

Characterization of the Flexiforce Signal Output

Typical response to harmonic excitation of the Flexiforce sensor is represented in Fig. 13. The minimum value $U_{\min}$ of the sinusoidal response is described by the static model introduced in (1). An exponential curve is used to fit the decrease of the maxima modeled by $U_{\max} = U_{\min} + ae^{-bt} + c$. After least-squares curve fitting, it is possible to estimate the RMSE by considering the n maxima of the sensor response on the time interval of the analysis

$$\text{RMSE} = \sqrt{\frac{\sum_{i=1}^{n}(\text{Max}_i - U_{\max}(t_i))^2}{n}} \tag{8}$$

with t_i the time instant when the maximum value Max_i occurs.

The quality of the model is estimated by computing relative errors on the parameters a, b, and c of the model, as well as by the MRE in the estimation of the maxima of the sensor response. To do so, the difference between the exponential decrease given by the model and the exponential curve fitted from the experimental data is computed for n values obtained after sampling

$$\text{MRE} = \frac{1}{n}\sum_{i=1}^{n}\frac{|U_{\max}(t_i) - U_{\text{model}}(t_i)|}{U_{\max}(t_i)}, \tag{9}$$

TABLE II
Variations of Parameters a, b, and c for the Flexiforce Sensor

Variations with f ($m = 2.7$N, $A = 1.5$N)

f (Hz)	0.05	0.15	0.25	0.50	1.00
a (V)	2.16	3.24	3.37	3.48	3.60
b (.10^3) (s^{-1})	4.32	7.46	5.57	7.01	7.07
c (V)	0.83	0.67	0.69	0.89	0.82
RMSE (V)	0.072	0.102	0.056	0.064	0.083
f (Hz)	1.50	2.00	2.50	3.00	4.00
a (V)	2.87	2.00	3.13	4.06	2.38
b (.10^3) (s^{-1})	8.10	5.57	12.2	18.9	8.57
c (V)	0.63	0.82	0.53	0.45	0.59
RMSE (V)	0.061	0.079	0.039	0.091	0.062

Variations with A ($m = 2.4$N, $f = 0.5$Hz)

A (N)	0.44	0.98	1.23	1.47	1.76
a (V)	0.44	1.98	2.19	3.39	4.19
b (.10^3) (s^{-1})	9.04	8.47	7.56	5.13	4.85
c (V)	0.29	0.67	0.73	0.48	0.47
RMSE (V)	0.006	0.043	0.053	0.076	0.053

Variations with m ($f = 0.5$Hz, $A = 0.8$N)

m (N)	1.77	1.96	2.45	2.94	3.43
a (V)	1.86	1.73	1.29	1.07	1.14
b (.10^3) (s^{-1})	6.76	6.18	6.79	8.35	7.27
c (V)	0.56	0.53	0.57	0.38	0.52
RMSE (V)	0.063	0.064	0.023	0.027	0.026

TABLE III
Relative Errors (in Percentage) of a, b, and c for a Sum of Two Sinusoidal Signals With Frequencies f_1, f_2 (in Hertz)
($A_1 = A_2 = 0.5$ N, $m = 2$ N)

f_1	0.33	0.08	0.5	0.5	0.1	0.05	0.02	0.01	0.01
f_2	0.5	0.2	1.5	2	0.5	0.5	0.5	0.5	1
a	37	41	41	19	26	17	25	33	13
b	8	11	36	9	45	30	92	15	37
c	4	9	14	3	11	13	7	4	8

References

[1] C. Lebossé, P. Renaud, B. Bayle, and M. de Mathelin, “Nonlinear modeling of low cost force sensors,” in *Proc. IEEE Int. Conf. Robot. Autom.*, Pasadena, CA, 2008, pp. 3437–3442.

[2] E. Dombre, G. Duchemin, P. Poignet, and F. Pierrot, “Dermarob: A safe robot for reconstructive surgery,” *IEEE Trans. Robot. Autom.*, vol. 19, no. 5, pp. 876–884, Oct. 2003.

[3] C. Lebossé, P. Renaud, B. Bayle, M. de Mathelin, O. Piccin, E. Laroche, and J. Foucher, “Robotic image-guided transcranial magnetic stimulation,” in *Computer Assisted Radiology and Surgery*. Berlin, Germany: Springer Verlag, 2006, pp. 137–139.

[4] J. Pires, “New challenges for industrial robot programming,” *Ind. Robot*, vol. 36, no. 1, p. 5, 2009.

[5] K. Hoshino and I. Kawabuchi, “Stable pinching with fingertips in humanoid robot hand,” in *Proc. IEEE Int. Conf. Intell. Robots Syst.*, Edmonton, AB, Canada, 2005, pp. 4149–4154.

[6] N. Maalej, S. Bhat, H. Zhu, J. Webster, W. Tompkins, J. Wertsch, and P. Bach-y Rita, “A conductive polymer pressure sensor,” in *Proc. Int. Conf. IEEE Eng. Med. Biol. Soc.*, New Orleans, LA, 1988, pp. 770–771.

[7] N. Maalej, J. Webster, W. Tompkins, and J. Wertsch, “A conductive polymer pressure sensor array,” in *Proc. IEEE Conf. Eng. Med. Biol. Soc.*, Seattle, WA, 1989, pp. 1116–1117.

[8] D. Bloor, K. Donnelly, P. J. Hands, P. Laughlin, and D. Lussey, "A metal-polymer composite with unusual properties," *J. Phys. D: Appl. Phys.*, vol. 38, no. 16, pp. 2851–2860, 2005.

[9] A. Balakrishnan, D. Kacher, A. Slocum, C. Kemper, and S. Warfield, "Smart retractor for use in image guided neurosurgery," in *Proc. Summer Bioeng. Conf.*, Key Biscayne, FL, 2003, pp. 895–896.

[10] K. Chinzei and K. Miler, "MRI guided surgical robot," in *Proc. Australian Conf. Robot. Autom.*, Sydney, Australia, 2001, pp. 50–55.

[11] D. Castro, L. Marques, U. Nunes, and A. de Almeida, "Tactile force control feedback in a parallel jaw gripper," in *Proc. IEEE Int. Symp. Ind. Electron.*, Guimarães, Portugal, 1997, pp. 884–888.

[12] H. Zhang and N. Chen, "Control of contact via tactile sensing," *IEEE Trans. Robot. Autom.*, vol. 16, no. 5, pp. 482–495, Oct. 2000.

[13] L. Birglen and C. Gosselin, "Fuzzy enhanced control of an underactuated finger using tactile and position sensors," in *Proc. IEEE Int. Conf. Robot. Autom.*, Barcelona, Spain, 2005, pp. 2320–2325.

[14] F. Vecchi, C. Freschi, S. Micera, A. Sabatini, and P. Dario, "Experimental evaluation of two commercial force sensors for applications in biomechanics and motor control," presented at the Int. Funct. Electr. Stimul. Soc., Aalborg, Denmark, 2000.

[15] M. Ferguson-Pell, S. Hagisawa, and D. Bain, "Evaluation of a sensor for low interface pressure applications," *Med. Eng. Phys.*, vol. 22, no. 9, pp. 657–663, 2000.

[16] K. Bachus, A. DeMarco, K. Judd, D. Horwitz, and D. Brodke, "Measuring contact area, force, and pressure for bioengineering applications: Using Fuji film and Tekscan systems," *Med. Eng. Phys.*, vol. 28, no. 5, pp. 483–488, 2006.

[17] J. Pavlovic, Y. Takahashi, J. Bechtold, R. Gustilo, and R. Kyle, "Can the Tekscan sensor accurately measure dynamic pressures in the knee joint?" in *Proc. Annu. Meeting Amer. Soc. Biomech.*, Clemson, SC, 1993, pp. 135–136.

[18] J. Otto, T. Brown, and J. Callaghan, "Static and dynamic response of a multiplexed-array piezoresistive contact sensor," *Exp. Mech.*, vol. 39, no. 4, pp. 317–323, 1999.

[19] R. Lakes, *Viscoelastic Solids*. Boca Raton, FL: CRC, 1999.

[20] E. Komi, J. Roberts, and S. Rothberg, "Evaluation of thin, flexible sensors for time-resolved grip force measurement," *IMechE Part C: J. Mech. Eng. Sci.*, vol. 221, pp. 1687–1699, 2007.

[21] (2009). [Online]. Available: http://www.tekscan.com/pdf/FlexiForce-Sensors-Manual.pdf

[22] (2011). [Online]. Available: http://www.interlinkelec.com/Force-Sensing-Resistor

[23] *Installation and Operations Manual for Stand-Alone F/T Sensor Systems*, ATI Industrial Automation, Inc., Apex, NC, 1997.

Keeping Multiple Moving Targets in the Field of View of a Mobile Camera

Nicholas R. Gans, Guoqiang Hu, Kaushik Nagarajan, and Warren E. Dixon

***Abstract*—This study introduces a novel visual servo controller that is designed to control the pose of the camera to keep multiple objects in the field of view (FOV) of a mobile camera. In contrast with other visual servo methods, the control objective is not formulated in terms of a goal pose or a goal image. Rather, a set of underdetermined task functions are developed to regulate the mean and variance of a set of image features. Regulating these task functions inhibits feature points from leaving the camera FOV. An additional task function is used to maintain a high level of motion perceptibility, which ensures that desired feature point velocities can be achieved. These task functions are mapped to camera velocity, which serves as the system input. A proof of stability is presented for tracking three or fewer targets. Experiments of tracking eight or more targets have verified the performance of the proposed method.**

***Index Terms*—Robust control, visual servoing, video surveillance.**

I. Introduction

Many vision-related control tasks cannot be formulated in terms of a specific goal pose or trajectory. Therefore, classical visual servoing methods (e.g., [1] and [2]) are not well suited to these problems. One task that is not well characterized by a goal pose or image is keeping multiple, moving objects in the camera field of view (FOV). Consider the scenario of crowd surveillance. A camera views the crowd and utilizes target segmentation and tracking methods to localize individuals of interest visible in the image. As the crowd moves and disperses, a controller must move and/or aim the camera in an attempt to keep all individuals in the FOV. Another scenario involves tracking several unmanned vehicles amid landmarks. Commands can be sent to the unmanned vehicles to track desired trajectories and avoid obstacles, but the vehicles must also be kept in the camera FOV to ascertain their pose in the workspace.

This paper presents a method to achieve the aforementioned tasks, extending our previous work in [3] and [4]. The method is rooted in classic image-based visual servoing [1], [2], [5], [6]; however, no goal image or goal feature trajectory is required. Rather than regulate error signals that are based on current and goal images, the proposed method regulates functions of the current image features. These task functions

Manuscript received February 9, 2011; accepted May 28, 2011. Date of publication June 30, 2011; date of current version August 10, 2011. This paper was recommended for publication by Associate Editor E. Marchand and Editor B. J. Nelson upon evaluation of the reviewers' comments. This work was supported in part by the Air Force Office of Scientific Research under Contract F49620-03-1-0381 and under Contract F49620-03-1-0170, in part by the Air Force Research Laboratory under Contract FA4819-05-D-0011, and in part by the U.S. Department of Energy under Grant DE-FG04-86NE37967. This work was accomplished as part of the DOE University Research Program in Robotics. This work was performed, in part, while N. Gans held a National Research Council Research Associateship Award at the Air Force Research Laboratory.

N. R. Gans and K. Nagarajan are with the Department of Electrical Engineering, University of Texas at Dallas, Richardson, TX 75080 USA (e-mail: ngans@utdallas.edu; kxn094020@utdallas.edu).

G. Hu is with the Department of Mechanical and Nuclear Engineering, Kansas State University, Manhattan, KS 66506 USA (e-mail: gqhu@ksu.edu).

W. E. Dixon is with the Department of Mechanical and Aerospace Engineering, University of Florida, Gainesville, FL 32611 USA (e-mail: wdixon@ufl.edu).

Color versions of one or more of the figures in this paper are available online at http://ieeexplore.ieee.org.

Digital Object Identifier 10.1109/TRO.2011.2158695